energies

MDPI

Article

Cenozoic Depositional Evolution and Stratal Patterns in the Western Pearl River Mouth Basin, South China Sea: Implications for Hydrocarbon Exploration

Entao Liu [1,*], Yong Deng [2,3,*], Xudong Lin [1], Detian Yan [4], Si Chen [4] and Xianbin Shi [5]

[1] Hubei Key Laboratory of Marine Geological Resources, China University of Geosciences, Wuhan 430074, China
[2] School of Geophysics, China University of Petroleum (Beijing), Beijing 102249, China
[3] Zhanjiang Branch Company, China National Offshore Oil Corporation, Zhanjiang 524057, China
[4] Key Laboratory of Tectonics and Petroleum Resources, Ministry of Education, China University of Geosciences, Wuhan 430074, China
[5] Hubei Geological Survey Institute, Wuhan 430030, China
* Correspondence: liuentao@cug.edu.cn (E.L.); dengy@cnooc.com.cn (Y.D.); Tel./Fax: +86-27-67886151 (E.L.)

Abstract: Investigating the deposition evolution and stratal stacking patterns in continental rift basins is critical not only to better understand the mechanism of basin fills but also to reveal the enrichment regularity of hydrocarbon reservoirs. The Pearl River Mouth Basin (PRMB) is a petroliferous continental rift basin located in the northern continental shelf of the South China Sea. In this study, the depositional evolution process and stacking pattern of the Zhu III Depression, western PRMB were studied through the integration of 3D seismic data, core data, and well logs. Five types of depositional systems formed from the Eocene to the Miocene, including the fan delta, meandering river delta, tidal flat, lacustrine system, and neritic shelf system. The representative depositional systems changed from the proximal fan delta and lacustrine system in the Eocene–early Oligocene, to the tidal flat and fan delta in the late Oligocene, and then the neritic shelf system in the Miocene. The statal stacking pattern varied in time and space with a total of six types of slope break belts developed. The diversity of sequence architecture results from the comprehensive effect of tectonic activities, sediment supply, sea/lake level changes, and geomorphic conditions. In addition, our results suggest that the types of traps are closely associated with stratal stacking patterns. Structural traps were developed in the regions of tectonic slope breaks, whereas lithological traps occurred within sedimentary slope breaks. This study highlights the diversity and complexity of sequence architecture in the continental rift basin, and the proposed hydrocarbon distribution patterns are applicable to reservoir prediction in the PRMB and the other continental rift basins.

Keywords: depositional system; sequence architecture; stacking pattern; Pearl River Mouth Basin; hydrocarbon exploration

check for updates

Citation: Liu, E.; Deng, Y.; Lin, X.; Yan, D.; Chen, S.; Shi, X. Cenozoic Depositional Evolution and Stratal Patterns in the Western Pearl River Mouth Basin, South China Sea: Implications for Hydrocarbon Exploration. *Energies* **2022**, *15*, 8050. https://doi.org/10.3390/en15218050

Academic Editors: Mohammad Sarmadivaleh and Shu Tao

Received: 18 September 2022
Accepted: 27 October 2022
Published: 29 October 2022

Publisher's Note: MDPI stays neutral with regard to jurisdictional claims in published maps and institutional affiliations.

Copyright: © 2022 by the authors. Licensee MDPI, Basel, Switzerland. This article is an open access article distributed under the terms and conditions of the Creative Commons Attribution (CC BY) license (https://creativecommons.org/licenses/by/4.0/).

1. Introduction

The continental rift basin is one of the most significant types of petroliferous basins. Approximately 31% of oil and gas fields in the world are distributed in continental rift basins with proven reserves of over 0.68×10^8 of oil equivalents [1]. Major petroleum systems sourced by Cenozoic sediments occur in a large number of sedimentary basins such as the Kachchh Basin (India), Congo Basin (Africa), Madrid Basin (Spain), Songliao Basin (China), and the basins in the South China Sea [1,2]. Investigation of the deposition evolution process in continental rift basins is critical to locating hydrocarbon reservoirs and predicting potential source rocks [2–6].

In sedimentary basins, stratigraphic and depositional architectures are fundamentally controlled by basin and tectonic evolution [7,8]. The dynamic process of basin filling is

mainly controlled by the interaction between sea/lake-level changes, tectonic subsidence, sediment supply, and geomorphic conditions, but the main controlling factor varies in different types of sedimentary basins [9–13]. In continental rift basins, tectonics is the most significant factor controlling depositional processes, including episodic rifting, differential subsidence, and the evolution and linkage of normal faults [4,14–19]. It exerts significant control on sedimentary fills, sequence architecture, and sand dispersal patterns [8,20–24]. By contrast, in marine basins, sequence stratal patterns and depositional architecture are mainly controlled by eustatic sea-level changes [9,10,25–27]. Even in a single basin, different evolutionary stages are characterized by different stratigraphic and depositional architectures [28,29]. For example, in continental rift basins, episodic tectonic subsidence with short stages of accommodation creation in response to pulses of fault reactivation usually occurs in the early stage, while little accommodation is generated due to tectonic quiescence, and sediment supply consumes and fills the available space in the later stage [2,5,8,30,31].

The tectono-stratigraphic archive provides unique insights into the evolution of stratigraphic and depositional architectures in continental rift basins [5,31–35]. Various palaeogeographic features formed by syn-depositional faults are getting more concern since they play a significant effect in the transportation and deposition of sediments [36–38]. Structural slope breaks are important types of palaeogeographic features, controlling the distribution of deposition systems through changes in the accommodation [33,36,39,40]. Overall, the previous studies related to stratigraphic and depositional architecture mainly focused on marine basins. For the continental rift basins, attention has been mainly paid to the rifting stage of continental rift basins [32,33,41,42]. However, studies on the evolutionary features during the long-time process are rare, especially for the evolutionary process from lacustrine to marine environments [22].

The Pearl River Mouth Basin (PRMB) is a significant hydrocarbon-bearing basin located in the central region of the northern margin of the South China Sea continental shelf [43–45]. It is a focus point for intensive hydrocarbon resources exploration because of the high petroleum potential in the Eocene–Miocene interval revealed by recent drilling findings [46,47]. The previous studies show that PRMB has undergone complex structural evolution from the lacustrine environment in the Eocene to the marine environment in the Miocene [48,49]. During the evolution process, multiple types of depositional systems (e.g., lacustrine system, neritic system, fan delta) were developed with great variability in time and space [49,50]. Although previous studies [46,47,51] have investigated the tectonic evolution, depositional systems, and source rock potential of the PRMB, rare study has focused on the depositional evolution and sequence filling processes during the basin evolution from lacustrine to marine environments, and the controlling factors for the sequence architecture and depositional system distribution remain debatable [42]. Moreover, the characteristics, spatial and temporal distribution, and evolutionary process of stratal stacking patterns in different stages of basin evolution are not clear. Given the above disputes over the depositional evolution of the PRMB, this study was conducted with the following aims: (1) to describe the evolution of depositional systems from the Eocene to the Miocene within a sequence stratigraphic framework; (2) to identify and characterize stratal stacking patterns in different basin evolutionary stages; (3) to investigate the characteristics of stratigraphic and depositional architecture throughout the entire history of basin filling; (4) to discuss the controlling factors for basin evolution and sediment filling process. Our study can not only enhance the understanding of sequence filling and depositional evolution processes in the continental rift basins from lacustrine to marine environments, but also serve as a new example for further exploration in the PRMB and the other basins in the South China Sea.

2. Geological Setting

The Pearl River Mouth Basin (PRMB) is a passive margin Cenozoic basin located in the center area of the northern continental margin of the South China Sea [45,52,53]. It covers

an area of approximately 26.7 × 10^4 km^2 and consists of four depressions from west to east, including the Zhu I Depression, Zhu II Depression, Zhu III Depression, and Chaoshan Depression (Figure 1A). The target study area, the Zhu III Depression, is located in the western region of the PRMB, covering a region of 12,180 km^2 with a water depth of 0–400 m. The Zhu III Depression is bounded by the South China Block to the north, Xisha Island to the south, Hainan Island to the west, and Taiwan Island to the east (Figure 1A). It consists of several subsidence centers (i.e., Wenchang A, B, C, D, and E Sags, Qionghai Sag, Yangjiang Sag) and structural highs (i.e., Qionghai Uplift, Shenhu Uplift, Yangjiang Uplift) (Figure 1B).

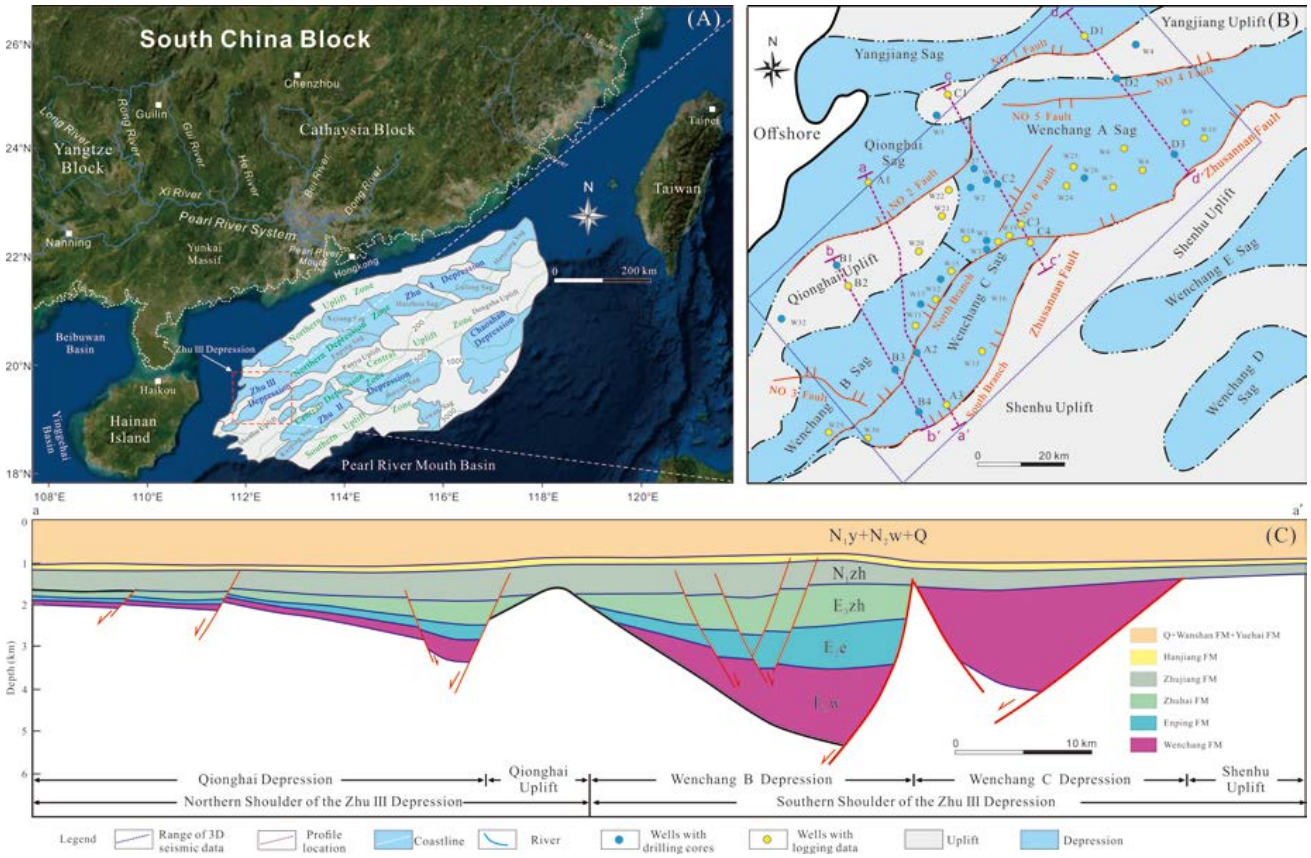


Figure 1. (**A**) Geological map of South China showing the regional setting and tectonic elements of the PRMB with major modern river systems that discharge into the northern South China Sea (modified after Liu et al. [50]). (**B**) Map showing tectonic elements of the Zhu III Depression and geographic locations of borehole samples. (**C**) Interpreted NE-trending profile in the Zhu III Depression and the location of the profile is shown in (**B**).

The Zhu III Depression has undergone a complex tectonic evolution associated with the continental rifting and evolution process of the South China Sea [52,54]. Its evolution history can be divided into four stages, including a pre-rifting stage (Shenhu Formation, 65–49 Ma), a rifting stage (Wenchang and Enping Formations, 39–30 Ma), a transition stage (Zhuhai Formation, 30–23.3 Ma), and a post-rifting stage (Zhujiang Formation, 23.3 Ma to present) (Figure 2). The Shenhu Formation (65–49 Ma) deposited during the pre-rifting stage and consisted of coarse-grained alluvial and volcanic deposits [49,52].

During the rifting stage (39–30 Ma), Wenchang (49–39 Ma) and Enping (39–30 Ma) Formations formed, and the depression is characterized by intense faulting and the development of several half-grabens [49,52,55]. The Wenchang and Enping Formations are represented by widespread terrestrial facies, including fan deltas and braided river deltas [55]. The boundary between the rifting stage and the transition stage was defined by the significant unconformity T_{70}, which is related to the regional Nanhai Event. The Oligocene Zhuhai Formation (30–23.3 Ma) that deposited during the transition stage with half-grabens

coalesced is mainly composed of tidal flats, semi-enclosed bays, and deltas [49,50,52]. The Miocene Zhujiang Formation (23.3–16.3 Ma) formed during the post-rifting stage when the PRMB began to receive marine sediments from the Miocene [50]. The Zhujiang Formation consists of fan delta and neritic deposits [49,52,56]. The source rocks are deposited in the Wenchang and Enping Formations, and the main reservoirs are located in the stratum of the Zhuhai and Zhujiang Formations. Several commercial oil pools were discovered in the central and marginal areas of the Wenchang A Sag [57].

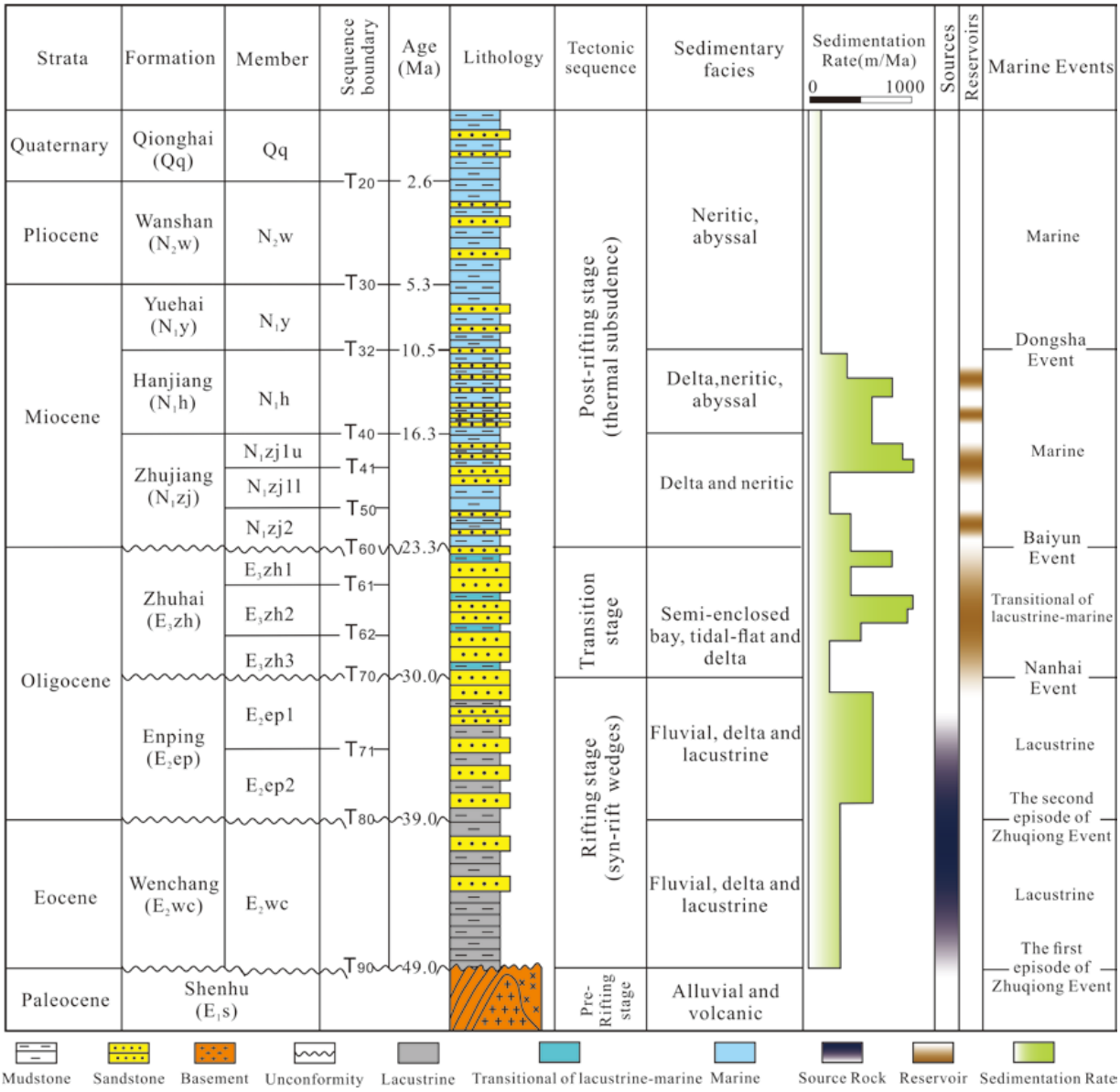


Figure 2. Generalized stratigraphic framework, sedimentary facies, tectonic evolution, and source-reservoir-cap assemblages of the PRMB. The sediment rate curve is from Xie et al. [49].

3. Material and Methods

3.1. Sequence Stratigraphic Framework

The combination of seismic data, drilling cores, logging data, and lithology data provided by CNOOC was used to conduct sedimentological and sequence stratigraphical studies. The seismic club comprises a region of approximately 2000 km^2, and its peak frequency is ~40 Hz. Seismic data were calibrated with well data using synthetic seismogram calibration. The sequence stratigraphic technique [9,58–60] was applied to establish a

sequence stratigraphic framework across the depression and to identify different stratal stacking patterns in different structural units.

3.2. Analysis of Sedimentary System

The types and ranges of depositional systems were determined using geological and geophysical methods [61,62]. Over 600 m of drilling cores from 20 wells were described to determine sedimentary facies and depositional characteristics. As drilling cores in the Zhu III Depression are limited, the logging and lithological association data from more than 50 wells, including natural gamma, true resistivity, and acoustic logging data, were also employed to identify depositional facies and to constrain their distribution ranges [40,63]. In no-well regions, the ranges of depositional systems were determined by 3D seismic data using seismic reflection, horizontal slice, and attributive analysis. The analysis of structural slope breaks was conducted based on seismic interpretation of 3D seismic data and analysis of sedimentary systems.

4. Results

4.1. Characteristics of Depositional Systems

Based on the comprehensive sedimentological analysis, five types of depositional systems were identified in the Zhu III Depression, western PRMB, including the fan delta, meandering river delta, tidal flat, neritic shelf system, and lacustrine system (Figures 3–5).

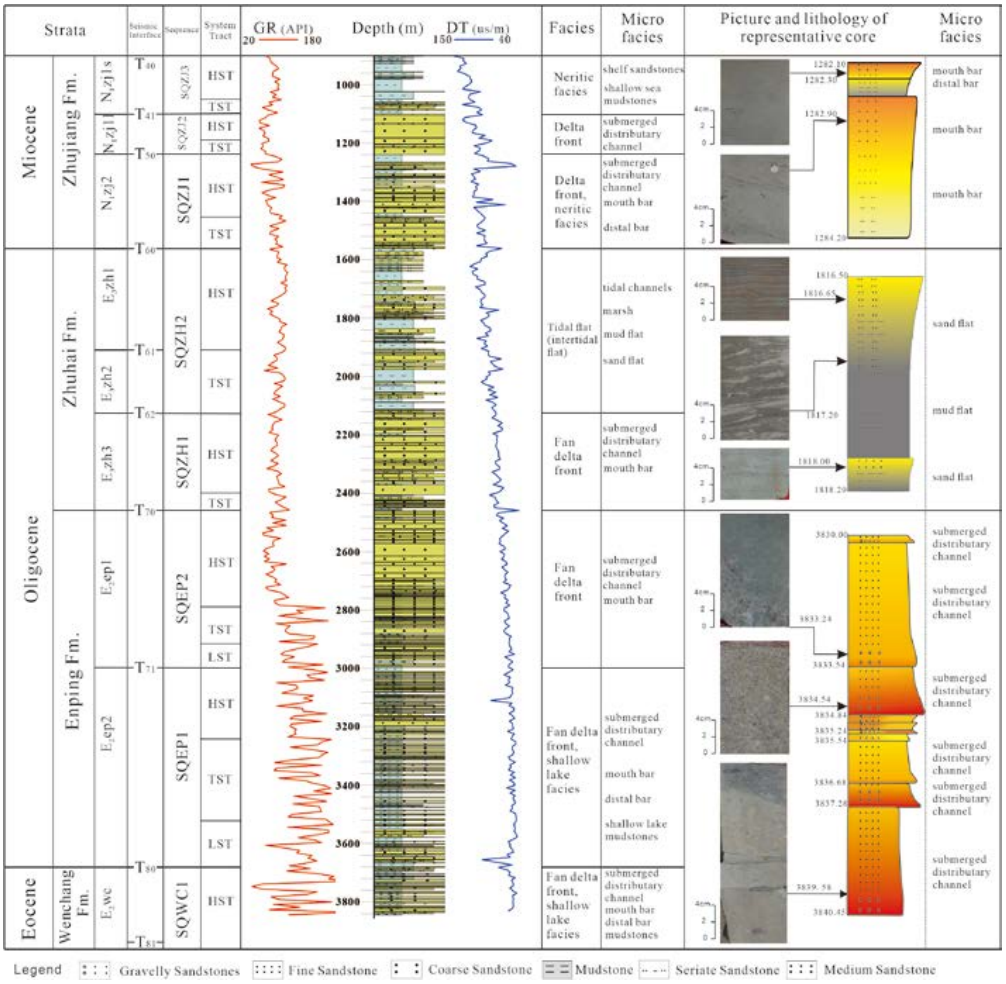


Figure 3. Drilling cores, logging, lithologic data, and interpreted depositional facies in Well A3 showing the depositional evolution from the Eocene to the Miocene. The location of Well A3 is shown in Figure 1.

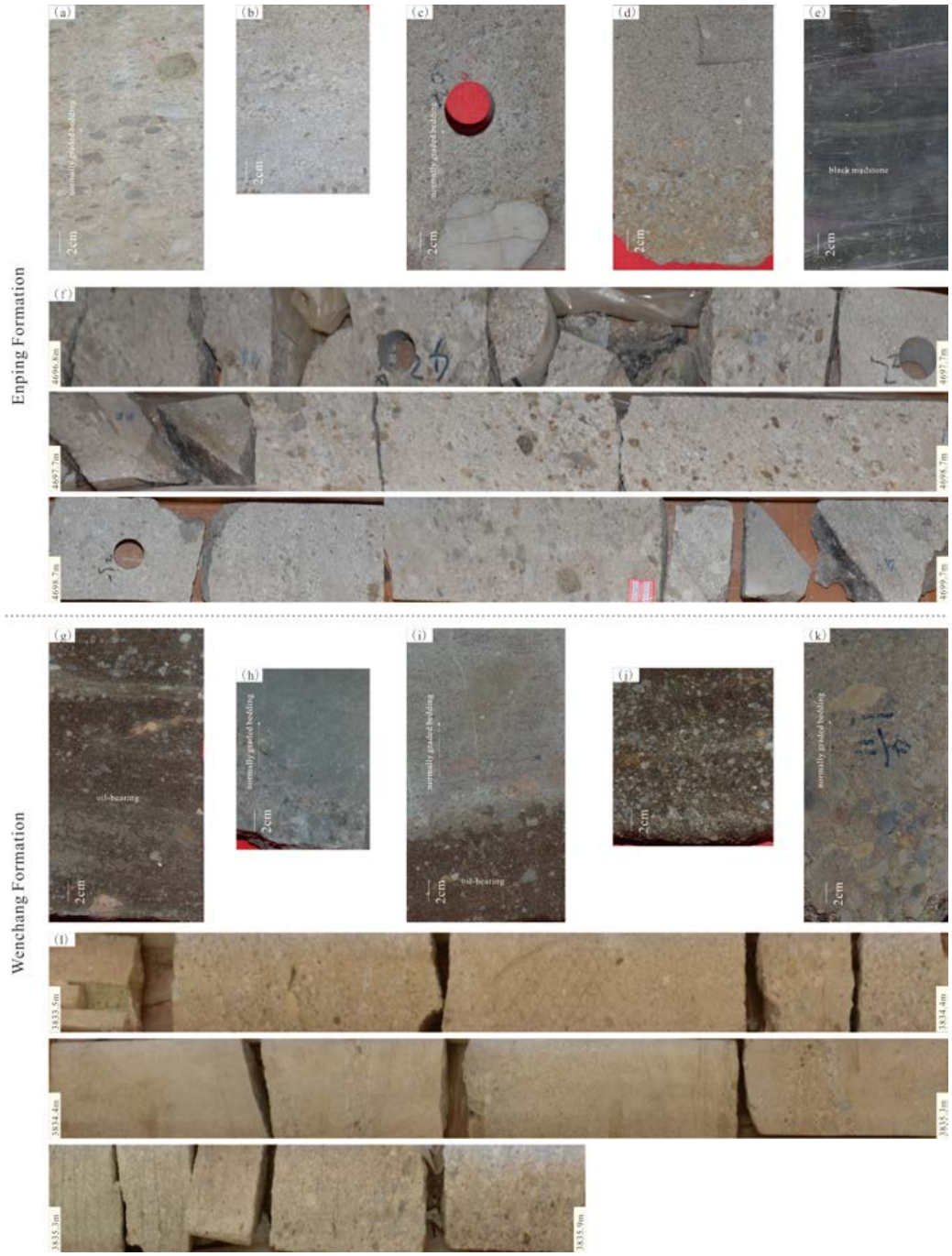


Figure 4. Typical sedimentary characteristics of the deposits in the Enping (**a**–**f**) and Wenchang (**g**–**l**) Formations in the Zhu III Depression: (**a**) 4694.4 m in Well W1, gravelly sandstone with normally graded bedding; (**b**) 4698.1 m in Well W1, gravelly sandstone; (**c**) 4695.4 m in Well W1, gravelly sandstone with normally graded bedding; (**d**) 4693.2m in Well W1, gravelly sandstone with normally graded bedding; (**e**) 4694.6 m in Well W1, black mudstone; (**f**) 2.9 m (4696.8–4699.7 m) long core of the underwater distributary channels of the fan deltas; (**g**) 4042.9 m in Well W13, oil-bearing gravelly sandstone; (**h**) 3830.0 m in Well B3, gravelly sandstone with normally graded bedding; (**i**) 3041 m in Well W12, oil-bearing gravelly sandstone with normally graded bedding; (**j**) 3043 m in Well 13, oil-bearing gravelly sandstone; (**k**) 3581 m in Well W9, gravelly sandstone; (**l**) 2.4 m (3833.5–3835.9 m) long core of the underwater distributary channels of the fan deltas.



Figure 5. Typical sedimentary characteristics of the deposits in the Zhujiang (**a**–**f**) and Zhuhai (**g**–**l**) Formations in the Zhu III Depression: (**a**) 2092.5 m in Well W4, siltstone; (**b**) 2092.8 m in Well W4, siltstone; (**c**) 2090.2 m in Well W4, fine-grained sandstone; (**d**) 2091.3 m in Well W4, fine-grained sandstone and siltstone with parallel bedding; (**e**) 1220.3 m in Well W32, fine-grained sandstone with normally graded bedding; (**f**) 2.0 m (2091.9–2092.9 m and 2093.9–2094.9 m) long core of the shallow-marine detrital deposits from the Zhujiang Formation; (**g**) 3210.7 m in Well W3, siltstone interbedded with mudstone; (**h**) 3210.9 m in Well W3, siltstone interbedded with mudstone; (**i**) 1861.2 m in Well A3, tidal rhythmites; (**j**) 1816.4 m in Well A3, tidal rhythmites; (**k**) 3211.1 m in Well W3, fine-grained sandstone interbedded with mudstone; (**l**) 3.0 m (3207.3–3210.3 m) long core of the tidal flat deposits in the Zhuhai Formation.

4.1.1. Fan Delta

The fan delta system consists of three sub-facies, including the fan delta plain, fan delta front, and pro-fan delta with the fan delta front being the most extensively distributed (Figure 6). Three lithofacies are recognized in the fan delta deposits (Figures 3 and 4): (a) gravelly sandstones with erosional bases, normally graded bedding, and widespread sandstone gravels (Figure 4a–d,g,j,k); (b) normally graded bedded sandstones with mud laminae at the top (Figure 4i,f,l); (c) thin fine-grained sandstones, siltstones with coarsening upward successions (Figure 4h,f,l).

Lithofacies (a) and (b) are interpreted as submerged distributary channels, which are funnel-shaped on the GR log, while lithofacies (c) are interpreted as distal bar deposits, which have a funnel-shaped geometry on the GR log (Figure 3). In the seismic profiles,

they are characterized by oblique progradational reflection configurations, low to medium continuous reflections, and medium to high amplitudes (Figures 7–9).

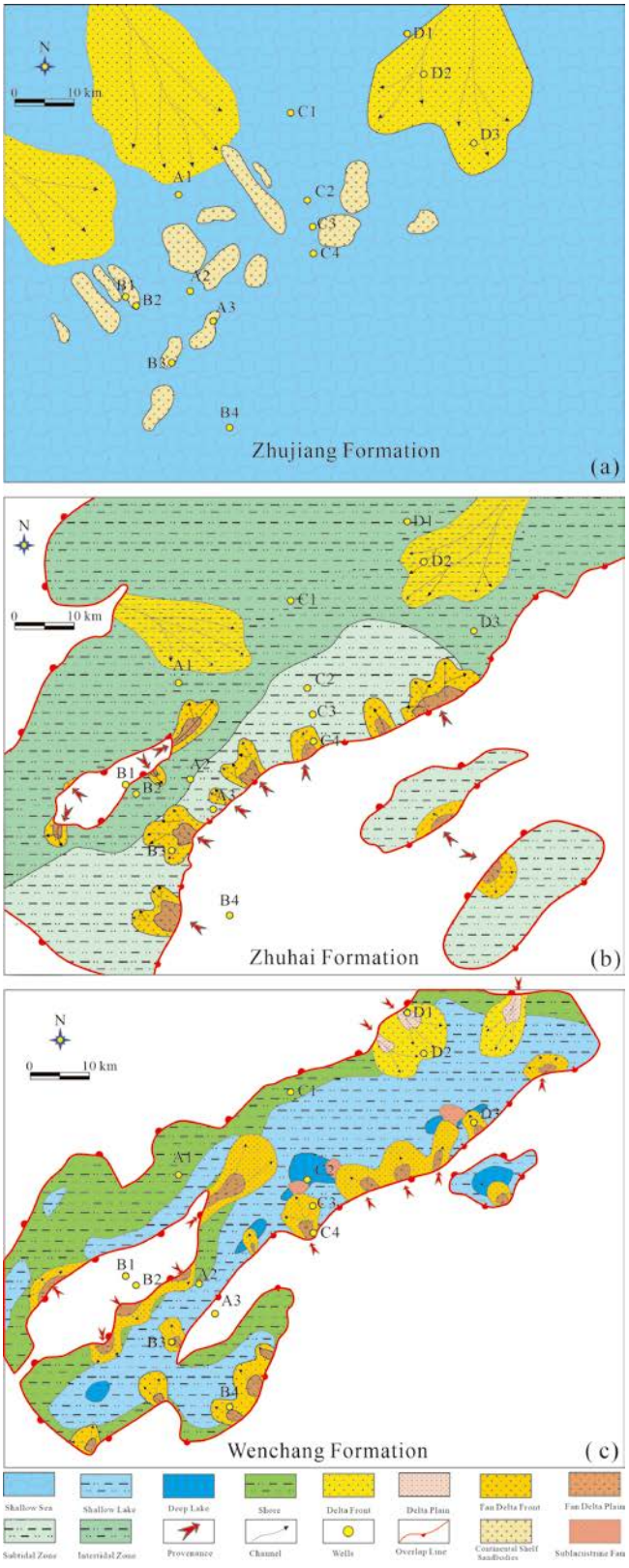


Figure 6. Deposition facies diagrams of the Zhujiang Formation (**a**), Zhuhai Formation (**b**), and Wenchang Formation (**c**) of the Zhu III Depression, PRMB, showing the depositional evolution from the Eocene Wenchang Formation to the Miocene Zhujiang Formation.

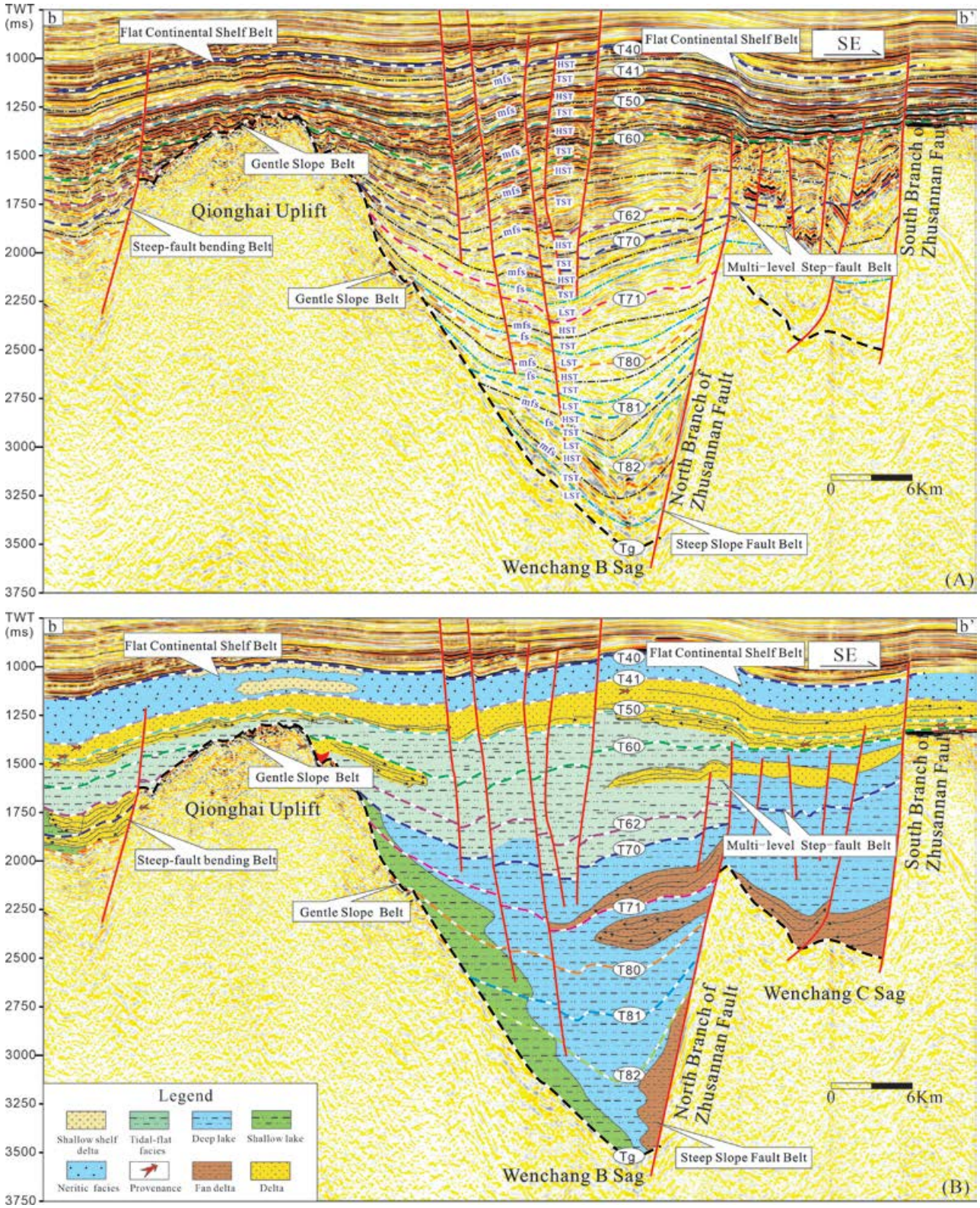


Figure 7. (**A**) interpreted seismic section bb′ showing seismic reflection characteristics and the distribution regions of different stratal stacking patterns; (**B**) the types of depositional facies and their distribution ranges in the section bb′ showing the depositional evolution from the Eocene to the Miocene. The location of section bb′ is shown in Figure 1.

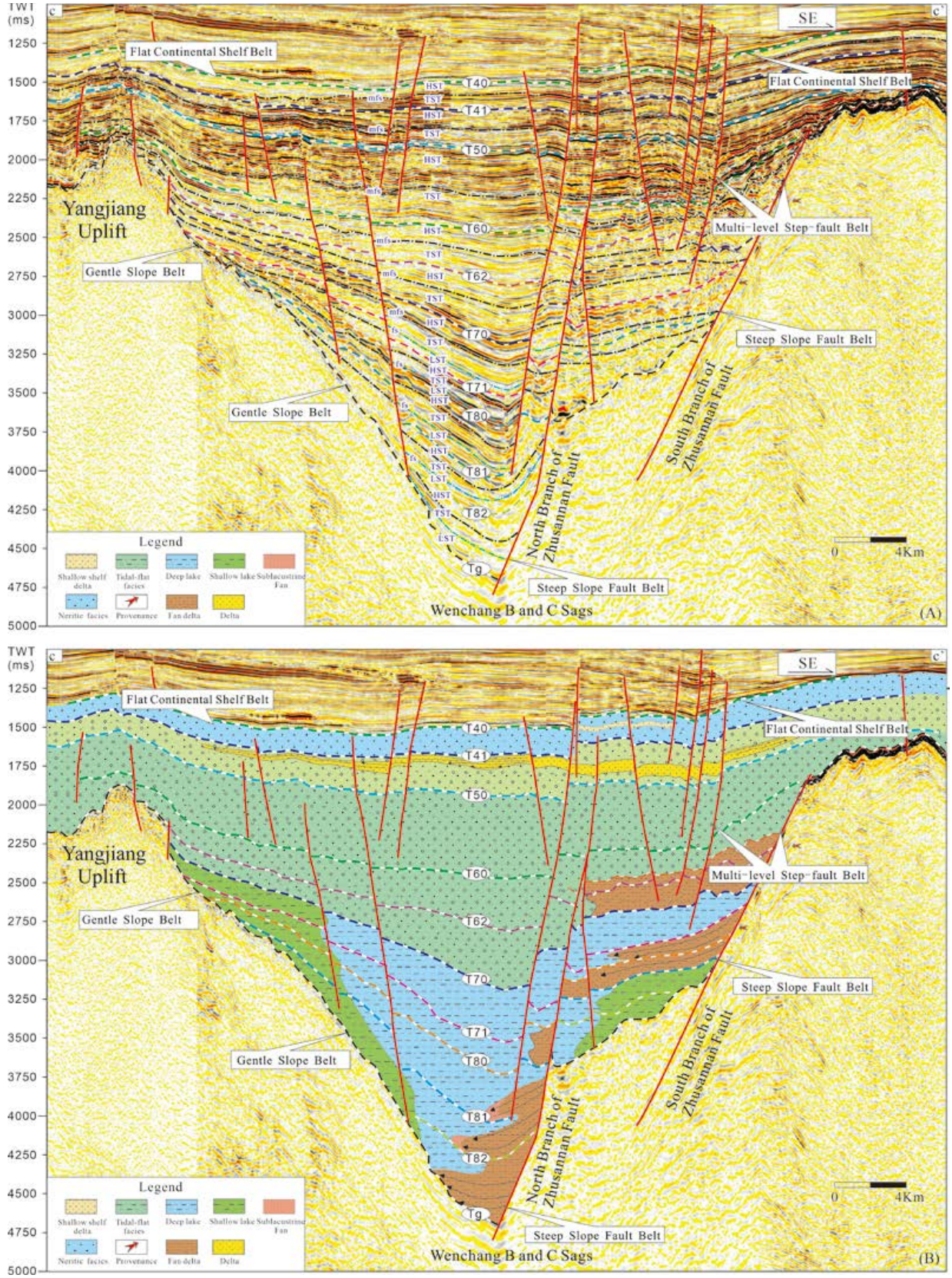


Figure 8. (**A**) interpreted seismic section cc′ showing seismic reflection characteristics and the distribution regions of different stratal stacking patterns; (**B**) the types of depositional facies and their distribution ranges in the section cc′ showing the depositional evolution from the Eocene to the Miocene. The location of section bb′ is shown in Figure 1.

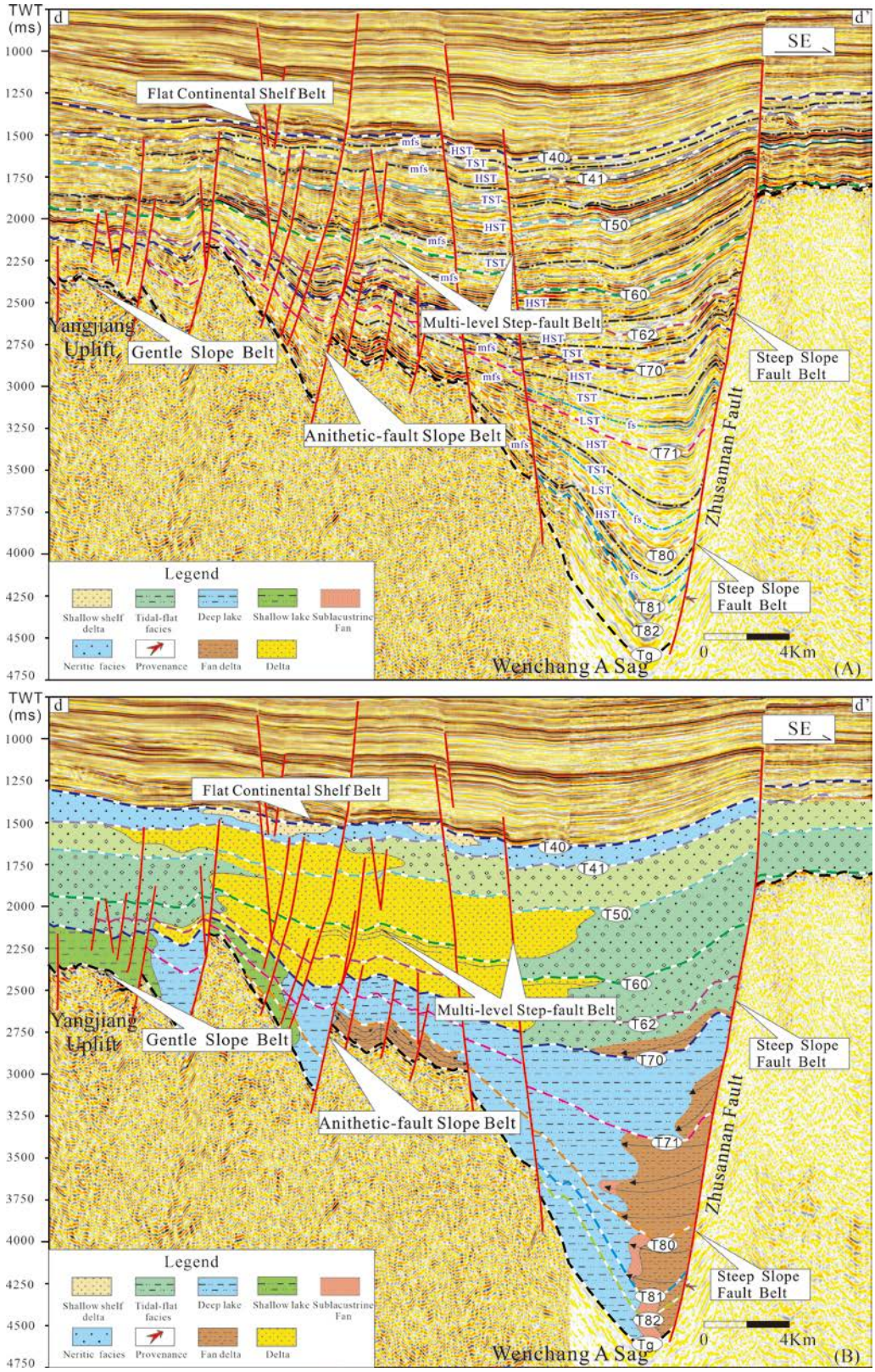


Figure 9. (**A**) interpreted seismic section dd′ showing seismic reflection characteristics and the distribution regions of different stratal stacking patterns; (**B**) the types of depositional facies and their distribution ranges in the section dd′ showing the depositional evolution from the Eocene to the Miocene. The location of section bb′ is shown in Figure 1.

Fan deltas are widely distributed in the Wenchang and Enping Formations, and are mainly located in the footwall blocks of the Zhusannan Fault as well as the adjacent region of the Qionghai Uplift in the Wenchang–Enping Formations (Figures 6 and 7). They exhibit fan-shaped plan view geometries and are distributed along the boundary faults.

4.1.2. Meandering River Delta

In contrast to fan delta deposits, meandering river delta deposits are significantly finer-grained with better sorting and roundness in detrital sediments (Figures 3 and 5a,b). The deposits are mainly composed of two lithofacies, including (a) normally graded bedded sandstones with mud laminae or mudstones at the top and (b) thin fine-grained sandstones, siltstones with coarsening upward successions (Figure 5b,c). Lithofacies (a) are interpreted as submerged distributary channels, whereas lithofacies (b) are interpreted as distal bars deposits.

Meandering river delta deposits are developed in the Zhu III Depression with their distribution ranges increasing from the Eocene to the Miocene (Figure 6). In the Wenchang–Enping Formations, meandering river delta deposits were confined to the northeast of the Zhu III Depression with their sediments from the Yangjiang Uplift (Figures 6, 8 and 9). In the later Oligocene Zhuhai Formation, meandering river delta deposits could be divided into two parts, including the northwestern delta system and the northeastern delta system (Figure 6). In the Miocene Zhujiang Formation, the distribution range of meandering river delta deposits further expanded (Figure 6).

4.1.3. Tidal Flat

The lithologies of tidal flat deposits are composed of siltstone, pelitic siltstone, fine-grained sandstone, and mudstone (Figures 3 and 5). Two types of lithofacies are developed including (a) siltstones interbedded with thin layers of mudstones (Figure 5g,h,k,l) and (b) tidal rhythmites that are characterized by packages of vertically accreted laminated to thinly bedded fine-grained sandstone and mudstone (Figure 5i,j,l).

Tidal flat deposits are widely distributed in the Oligocene Zhuhai Formation (Figures 6–9). Two types of sub-facies are identified in the Zhu III Depression, including the intertidal zone and the subtidal zone. The intertidal zone was developed in the northern depression ranging from Yangjiang Sag to Wenchang B Sag, while the subtidal zone was distributed in the southern depression (i.e., Wenchang C, D, and E Sags) (Figure 6).

4.1.4. Lacustrine System

Lacustrine deposits are widely distributed in the Wenchang and Enping Formations and are composed of two sub-facies (i.e., the shallow-lacustrine and the deep-lacustrine deposits) (Figure 6). The deep-lacustrine deposits developed primarily in the centers of half-grabens, and the lithofacies consists of thick layers of gray-black mudstones. On the seismic profiles, the deep-lacustrine deposits display continuous, high-amplitude, high-frequency, and unparallel reflections (Figures 7–9). By contrast, the shallow-lacustrine deposits consist of thick gray mudstones interbedded with thin layers of fine-grained sandstones with small-scale cross-bedding and waving bedding (Figure 4e). The shallow-lacustrine deposits are characterized by divergent reflector configurations on seismic sections (Figures 7–9).

4.1.5. Neritic Shelf System

Neritic shelf deposits are developed only in the Miocene Zhujiang Formation (Figure 6). They are composed of two types of lithofacies: (a) thick black marine mudstones that contain bivalve, brachiopod shells; (b) massive fine-grained sandstones that are well-sorted and well-rounded (Figures 3 and 4f). Lithofacies (a) is interpreted as offshore black marine mudstone, and Lithofacies (b) is interpreted as the deposits of neritic shelf sand bodies. On the seismic profiles, the neritic shelf deposits display continuous, high-amplitude, high-frequency, and parallel reflections (Figures 7–9).

4.2. Sequence Architecture and Stacking Patterns

4.2.1. Sequence Stratigraphic Framework

Sedimentological and sequence stratigraphy analysis show that the sequence architecture in the Zhu III Depression varies in time and space (Figures 7–9). The Eocene Wenchang Formation is composed of three sequences, and the Oligocene Enping Formation is composed of two sequences [42]. These sequences consist of lowstand, transgressive, and highstand systems tracts (Figures 7–9). The lowstand systems tract is located in the centers of the deep lake, which is characterized by thick wedge-shaped progradation seismic reflection. The transgressive systems tract is characterized by medium, continuous parallel reflections, whereas the highstand systems tract features low-angle oblique progradation reflections (Figures 7–9). By contrast, the Oligocene Zhuhai Formation and the Miocene Zhujiang Formation consist of two and three sequences, respectively, composed of only transgressive and highstand systems tracts [42]. In the Oligocene Zhuhai Formation, the highstand systems tract displays strong amplitude and continuous reflection characteristics, while the transgressive systems tract shows moderate–weak amplitude on the seismic reflection (Figures 7–9). Different from the overlying strata, the third sequence (SQZJ3) in the Miocene Zhujiang Formation is composed of shallow-marine detrital deposits, and the continental shelf sand bodies are developed only within the highstand systems tract (Figure 3).

4.2.2. Depositional Stacking Patterns

Six types of slope break belts are identified in the Zhu III Depression (Figure 10), and their features are described as follows.

(1) Steep slope fault belt

The steep slope fault belt is defined as a steep slope that is controlled by a syn-sedimentary boundary fault (Figure 10). Such a boundary fault usually has a large fault displacement and a straight plan pattern (Figure 10). A deep fault terrace is developed at the footwall of the boundary fault where clastic sediments are accumulated (Figure 10). In the Zhu III Depression, the steep slope fault belt is mainly located at the footwalls of the Zhusannan Fault, which constitute the southwest margins of the Wenchang A, B, and C Sags (Figures 7–9 and 11).

(2) Steep-fault bending belt

The steep-fault bending belt features a steep slope that is controlled by both a syn-sedimentary boundary fault and a pre-existing uplift (Figure 10). Compared with the steep slope fault belt, the slope of the steep-fault bending belt is much gentler, and fault displacement is smaller, which is influenced by the pre-existing uplift (Figure 10). The steep-fault bending belt in the Zhu III Depression developed mainly along the footwall of the No.2 Fault, the north margin of the Qionghai Uplift (Figures 7–9 and 11).

(3) Multi-level step-fault belt

The multi-level step-fault belt is characterized by multiple fault terraces jointly controlled by several syn-sedimentary faults (Figure 10). These faults usually have a ladder-shaped profile and are parallel to each other (Figure 10). Each fault terrace is controlled by a single syn-sedimentary fault, creating an accommodation zone for sediment deposition (Figure 10). The multi-level step-fault belts are mainly located at the footwalls of the Zhusannan Fault and No.5 Fault during the sedimentary period of the Zhuhai Formation (Figures 7–9 and 11).

(4) Antithetic-fault slope belt

The antithetic-fault slope belt is featured by multiple fault terraces formed by the development of antithetic faults (Figure 10). The dip direction of antithetic faults is opposite to the direction of sediment transport, which is significantly different from the multi-level step-fault belt (Figure 10). In the Zhu III Depression, the antithetic-fault slope belt is only

located on the east margin of the Qionghai Uplift in the stratum of the Wenchang and Enping Formations (Figures 9 and 11).

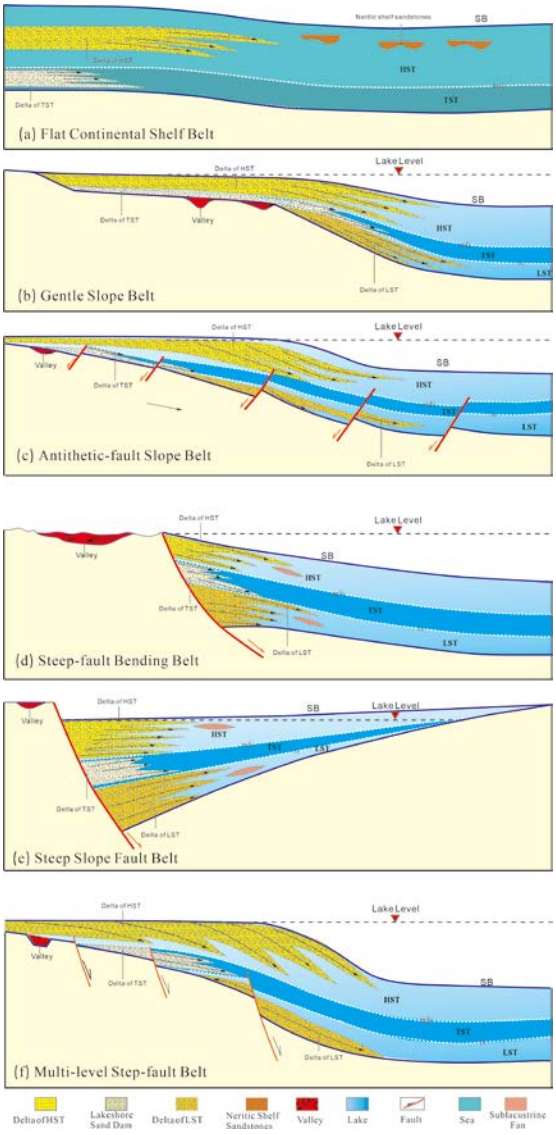


Figure 10. The types of slope break belts and their stratal stacking patterns in the Zhu III Depression, PRMB.

(5) Gentle slope belt

The gentle slope belt is characterized by limited change of slope gradient with a lack of intensive syn-sedimentary normal faults (Figure 10). The sediments are distributed and generally disappear along the slope (Figure 10). In the Zhu III Depression, the gentle slope belt is mainly located on the margins of the Qionghai and Yangjiang Uplifts during the depositional period from the Wenchang Formation to the Zhuhai Formation (Figures 7–9 and 11).

(6) Flat continental shelf Belt

The flat continental shelf belt is featured by a nearly horizontal stratum with a low angle of <2° (Figure 10). There is neither an intensive normal fault nor gentle slope (Figure 10). Long-distance transported sediments are deposited along the continental shelf as large-scale meandering river deltas (Figure 10). Neritic shelf sandstones are formed due to the modification of storms and tides (Figure 10). In the Zhu III Depression, the flat continental shelf belt is located almost in the whole depression during the depositional period of the Zhujiang Formation (Figures 7–9 and 11).

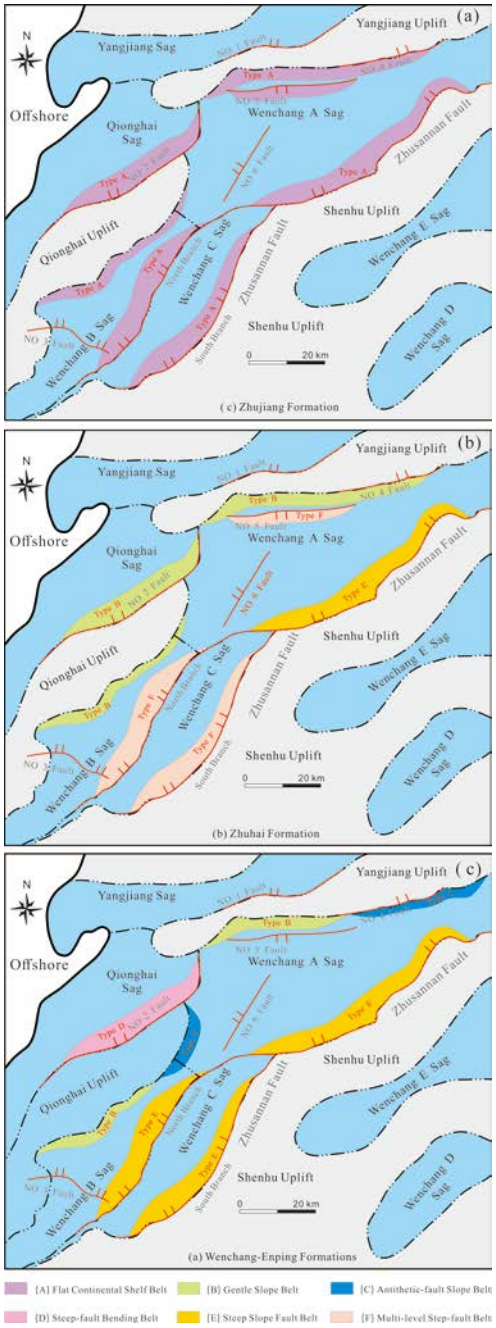


Figure 11. The spatial distributions of slope break belts of the Zhujiang Formation (**a**), Zhuhai Formation (**b**), and Wenchang-Enping Formations (**c**) in the Zhu III Depression, PRMB.

5. Discussion

5.1. Tectonic Controls on the Evolution of Depositional Systems

There are four stages in the tectonic evolution history of the Zhu III Depression, including the pre-rifting stage, rifting stage, transition stage, and post-rifting stage (Figure 2). Each evolutionary stage shows distinctive characteristics in basin configuration and stratigraphic architecture (Figures 6–9). During this evolution process, the representative depositional systems changed from proximal fan delta and lacustrine deposits in the Eocene Wenchang and Oligocene Enping Formations, to tidal flat and fan delta deposits in the Oligocene Zhuhai Formation, and then distal meandering river delta and neritic deposits in the Miocene Zhujiang Formation (Figure 6).

During the rifting stage, the basin is characterized by wedge-shaped geometries with the development of several NE trending half-grabens because of intense rifting (Figures 6–9). The structural highs developed along the basin margin and, among the half-grabens, acted as significant source areas for proximal fan delta deposits, which were accumulated mainly in the footwall scarps of boundary faults (Figures 7–9). During the transition stage, basin rifting was weakened, and the increase in subsidence of the PRMB led to large-scale transgression [56]. Tidal flats were widely developed during this stage, and the fan deltas were deposited at the footwalls of boundary faults. During the post-rifting stage, rifting was almost negligible, and the subsidence rate significantly weakened and gradually stabilized (Figures 6–9). As a result, the isolated sub-sages were gradually interconnected to form a unified depression, and the whole depression was covered by the shallow sea shelf (Figure 6). This consequently resulted in the formation of a structural foundation for the development of neritic shelf sandstones and long-distance transported deltas in the continental shelf (Figure 6). Therefore, it can be concluded that tectonic evolution controlled the basin configuration and evolution process of depositional systems.

Normal faults significantly control sequence architecture and syn-rift successions in extensional systems through the generation of accommodation space [33,41,64,65]. In the Zhu III Depression, the Zhusannan Fault was critical in controlling accommodation and the distribution of deposition systems (Figures 7–9). In different basin evolutionary stages, the Zhusannan Fault had different characteristics of fault activity and fault geometry, affecting the development position of sand bodies. During the rifting stage (Wenchang–Enping Formations), the Zhusannan Fault was marked by large displacement and a high activity rate (as high as 250 m/Ma) [42]. Because of the intensive faulting, the high steep slope topography was formed with the fault scarp directly adjoined to the deep lake (Figure 10). The root of the Zhusannan Fault was the largest accommodation space in the depression, providing a depositional site for the nearshore fan delta (Figures 7–9). In this stage, fan delta systems of different sizes were mainly distributed along the Zhusannan Fault with prograding stacking patterns (Figures 7–9).

By contrast, during the transition stage (Zhuhai Formation), the fault activity of the Zhusannan Fault significantly decreased to <100 m/Ma [42], and the subsidence centers gradually moved away from the footwalls of the Zhusannan Fault (Figures 7–9). In this stage, secondary syn-sedimentary faults that were parallel to the Zhusannan Fault were formed and maintained a tectonic low landform (Figures 7 and 8). These faults, together with the Zhusannan Fault, controlled the distribution ranges of fan delta systems (Figures 7 and 8). Compared with the fan deltas in the rifting stage, the distribution ranges of fan deltas are much smaller (Figures 6–9). During the post-rifting stage, the Zhusannan Fault exerted little effect on the distribution of deposition systems. The Shenhu Uplift was gradually submerged and unable to provide sediments to form fan deltas, while the large-scale meandering river delta sourced from the Pearl River in the north became the dominant deposition system [50]. In this stage, the distribution pattern of depositional systems was mainly controlled by sea-level change and sediment supply, which have been documented in previous studies [66].

In summary, the filling patterns and distribution of depositional systems were controlled by several factors (i.e., tectonic activities, sea-level change, and sediment supply), but the main controlling factor is not uniform during the basin evolution process from rifting stage to the post-rifting stage. In the rifting stage, the intense rifting of boundary faults significantly controlled the distribution of depositional systems, whereas sea-level change and sediment supply became significant controlling factors for stratigraphic architecture.

5.2. Sequence Architecture Evolution

Structural and sedimentary slope breaks have significant control over the distribution pattern of depositional systems [12,21,33,67]. Six types of slope break belts have been identified in the Zhu III Depression, exerting significant functions on stratal stacking patterns (Figure 10). The sequence architecture differs greatly in space and time (Figures 10 and 11).

For example, in the northern depression, the sequence architecture was mainly controlled by faulting, and two different faulting patterns (i.e., steep slope fault belt, multi-level step-fault belt) were developed during the evolving growth of the Zhusannan Fault (Figure 11). By contrast, the sequence architecture in the regions adjacent to the Qionghai Uplift in the western depression was mainly controlled by the gentle slope belt (Figure 11). Even in the regions along the footwall of the Zhusannan Fault, two different patterns, including the steep slope fault belt in the west and the multi-level step-fault belt in the east, were revealed in the depositional period of the Zhuhai Formation, indicating that the fault geometry (low-angle or high-angle) is also an important factor controlling the depositional patterns (Figure 11). Therefore, our results highlight the diversity and complexity of sequence architecture in the continental rift basin, which resulted from the comprehensive effect of sea/lake-level changes, faulting, palaeogeomorphology, and sediment supply.

The diversity and complexity of sequence architecture are closely associated with the tectonic evolution process [7,21,66]. The dynamic evolution process of sequence architecture can be divided into three stages: (1) During the rifting stage, the steep slope fault belt and steep-fault bending belt were developed in the footwalls of the Zhusannan and No.2 Fault, respectively (Figure 11). The antithetic-fault slope belt and gentle slope belt were developed around the uplifts (Figure 11). The depression was filled with widespread fan delta deposits on the gentle slopes and steep slopes (Figure 6). The distribution of fan deltas in the fault zones was mainly controlled by faulting, while that in the gentle slope was dominantly controlled by palaeogeomorphology (Figure 10). (2) During the transition stage, the steep slope fault belt developed in the footwall of the Zhusannan Fault converted into the multi-level step-fault belt, which controlled the distribution of sedimentary facies from the shallow to the deep lacustrine environment (Figures 7 and 8). By contrast, in the regions of the intrabasin uplifts (e.g., Qionghai Uplift), the previously developed filling patterns have changed to the gentle slope belt (Figure 11). (3) During the post-rifting stage, the end of tectonism caused the cessation of differential subsidence, and the previously developed sequence patterns were replaced by the flat continental shelf belt (Figures 6–9). The depositional systems and their stratal stacking patterns were dominantly controlled by sea-level change and sediment supply [66], and tectonic activities had little effect on the sequence architecture.

In summary, the spatial and temporal features of stratal stacking patterns varied with a single structural unit and between different structural units (Figure 11). From the rifting stage to the post-rifting stage, the dominant stacking patterns have changed from tectonic slope breaks (e.g., steep slope fault belt, steep-fault bending belt) to sedimentary slope breaks (e.g., flat continental shelf belt) (Figure 11). The diversity of sequence architecture resulted from the comprehensive effect of tectonic activities, sediment supply, sea/lake-level changes, and geomorphic conditions. The sequence architecture is mainly controlled by the tectonic activities in the rifting stages, whereas it is dominantly controlled by sediment supply and sea-level changes in the post-rifting stage.

5.3. Hydrocarbon Accumulation Rules and Exploration Direction

The basin evolution and sequence architecture can control not only the depositional filling process but also the distribution of hydrocarbon resources and the types of traps [33,68–70]. Structural traps are widely developed in the regions of tectonic slope breaks (e.g., steep slope fault belt, steep-fault bending belt, multi-level step-fault belt) where fault traps and faulted anticlinal traps formed (Figures 12 and 13). By contrast, lithological traps have a close relationship with the development of the sedimentary slope breaks (e.g., gentle slope belt, flat continental shelf belt) (Figures 12 and 13). There are two types of lithological traps, including up-dip wedge-out traps and lithologic lenticular traps (Figure 12), but their formation regions are different. Up-dip wedge-out traps were formed in the stratum of Wenchang, Enping, and Zhuhai Formations, whereas lithologic lenticular traps were developed mainly in the Zhujiang Formation (Figure 12). In addition, stratigraphic onlap

traps are developed by subsequent uplift and erosion, especially in the stratum of the Zhuhai Formation in the Qionghai Uplift (Figure 12).

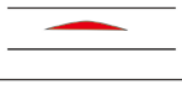
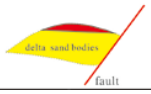
Trap Type	Hydrocarbon Reservoir Type	Model Diagram	Development Region	Development Strata
Lithologic Trap	Updip Wedge-out Trap		Qionghai Uplift	Enping, Zhuhai and Zhujiang Formations
			Wenchang Sag B	Wenchang and Enping Formations
	Lithologic Lenticular Trap		Wenchang Sag A and B	Zhujiang Formation (T40-T41)
			Wenchang Sag A and B	Wenchang and Enping Formations
Stratigraphic Trap	Stratigraphic Onlap Trap		Qionghai Uplift	Zhuhai Formation
			Wenchang Sag A	Zhuhai Formation
Structural Trap	Fault Trap		Zhusannan Fault No 2 Fault System No 6 Fault System No 5 Fault System	Wenchang, Enping, and Zhuhai Formations
	Faulted Anticlinal Trap		Wenchang Sag B	Zhuhai Formation

Figure 12. The types of traps and their development strata and regions in the Zhu III Depression, PRMB.

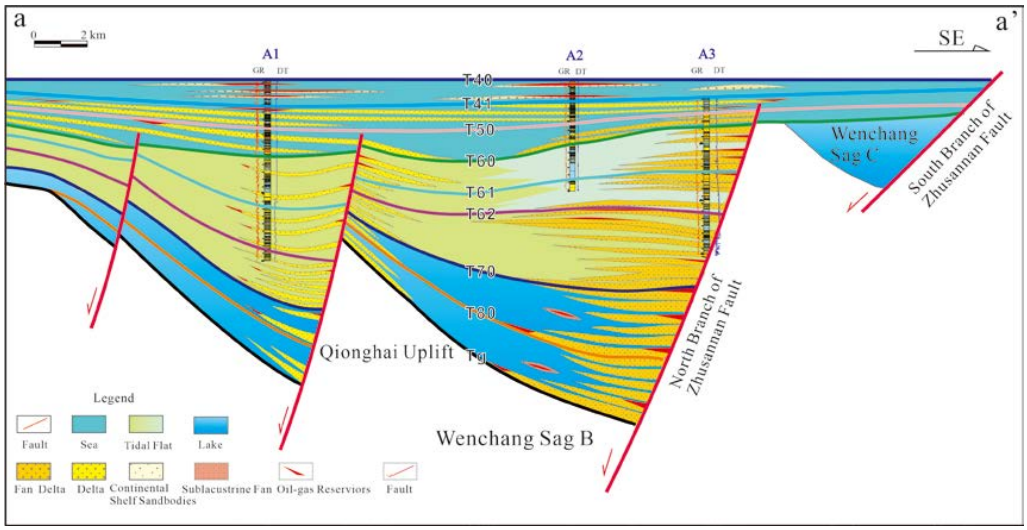


Figure 13. The type and distribution of oil and gas reservoirs across the representative section in the Zhu III Depression, PRMB. The location of section aa' is shown in Figure 1.

The sequence stacking pattern is closely associated with trap types and their distribution [68,69]. In the regions of steep slope fault belts and steep-fault bending belts, three different types of traps are developed, including fault traps at the fault terraces of the boundary faults, up-dip wedge-out traps in the north, and sublacustrine fan traps in the deep lake (Figure 13). In the multi-level step-fault belts, lobate sand bodies are deposited on each fault terrace where fault traps develop. In the gentle slope belts, up-dip wedge-out traps and lithologic lenticular traps are formed (Figure 13). By contrast, in the flat continental shelf belts, neritic shelf sand bodies developed in the Miocene Zhuhai Formation are favorable for forming lithologic lenticular traps (Figure 13).

In the last few decades, exploration achievements have been mainly achieved in the regions of structural traps [71]. The investigation of depositional evolution and stratal stacking patterns provides valuable insights into guiding the exploration and development [33,68,69]. According to exploration status and characteristics of trap distribution, the hydrocarbon exploration in the Zhu III Depression should be conducted at different levels: (1) The flat continental shelf belt developed in the Miocene Zhujiang Formation should be the most

significant area for future exploration since the neritic shelf sand bodies distributed in the flat continental shelf are characterized by a high-quality reservoir property with average porosity and permeability values higher than 18% and 140 mD, respectively. The oils in the sandstone reservoirs are high maturity (Ro = 0.8~1.3%) and originated from the Enping Formation (Toc = 1.6~2.4%, HI = 233~332 mg/g TOC) [71]. Moreover, the neritic shelf sand bodies are favourable for forming "self-reservoir and self-coverage" lithologic reservoirs (Figure 13). Moreover, compared with the other traps, the hydrocarbon exploration for the neritic shelf sand bodies faces fewer difficulties, such as shallow burial, low exploration cost, and good seismic quality. These advantages profoundly influence the hydrocarbon enrichment and increase the success rate of hydrocarbon exploration, but determining the distribution range of neritic shelf sand bodies is primary. (2) The gentle slope belt in the adjacent region of the Qionghai Uplift should be an important area for future exploration (Figure 13). The up-dip wedge-out traps in this region are key exploration targets for seeking lithologic reservoirs. (3) The steep slope breaks (i.e., steep slope fault belt, steep-fault bending belt) located in the footwalls of the Zhusannan Fault should be scientifically investigated to achieve breakthroughs (Figure 13). The primary difficulty in these regions is poor seismic data quality, and more study is needed before locating an exploration target.

6. Conclusions

During the basin evolution process from the rifting stage to the post-rifting stage in the western Pearl River Mouth Basin (PRMB), in the northern South China Sea, five types of depositional systems were developed, including the fan delta, meandering river delta, tidal flat, lacustrine system, and neritic shelf system. The representative depositional systems changed from the proximal fan delta and lacustrine system in the Eocene–early Oligocene, to the tidal flat and fan delta in the late Oligocene, and then the neritic shelf system in the Miocene. The intense rifting of boundary faults significantly controlled the distribution of depositional systems in the rifting stage, whereas sea-level change and sediment supply became significant controlling factors for stratigraphic architecture in the post-rifting stage.

Six types of slope break belts (i.e., steep slope fault belt, steep-fault bending belt, multi-level step-fault belt, antithetic-fault slope belt, gentle slope belt, flat continental shelf belt) developed in the western PRMB, which exerted significant functions on stratal stacking patterns. Our results highlight the diversity and complexity of sequence architecture in the continental rift basin, which resulted from the comprehensive effects of sea/lake-level changes, faulting, palaeogeomorphology, and sediment supply.

Stratal stacking patterns are closely associated with trap types and their distribution. According to the exploration status and characteristics of trap distribution, the hydrocarbon exploration in the Zhu III Depression should be conducted at different levels: the flat continental shelf belt and the gentle slope belt are recommended as the key targets for exploration, whereas the steep slope break belt requires further investigations to achieve breakthroughs.

Author Contributions: Conceptualization, E.L. and Y.D.; methodology, S.C.; software, X.L.; validation, D.Y.; formal analysis, S.C.; investigation, X.S.; resources, Y.D.; data curation, X.S.; writing—original draft preparation, E.L.; writing—review and editing, S.C.; visualization, D.Y.; supervision, Y.D.; project administration, Y.D. and D.Y.; funding acquisition, E.L. All authors have read and agreed to the published version of the manuscript.

Funding: This work was supported by the National Natural Science Foundation of China (Nos. 42072142, 41702121, U19B2007).

Data Availability Statement: Not applicable.

Acknowledgments: We appreciate Zhanjiang Branch Company of China Offshore Oil Corporation for providing the data and permission to publish this paper. We are also very grateful to the reviewers and editors for their contributions to improving this paper.

Conflicts of Interest: The authors declared that they have no conflict of interest in this work. We declare that we do not have any commercial or associative interest that represents a conflict of interest in connection with the work submitted.

References

1. Dou, L.R.; Pan, X.H.; Tian, Z.J.; Xiao, K.Y.; Zhang, Z.W. Hydrocarbon formation and distribution of rift basins in Sudan: A comparative analysis of them with rift basins in East China. *Pet. Explor. Dev.* **2006**, *33*, 255–261.
2. Martins-Neto, M.A.; Catuneanu, O. Rift sequence stratigraphy. *Mar. Pet. Geol.* **2010**, *27*, 247–253. [CrossRef]
3. Maravelis, A.G.; Chamilaki, E.; Pasadakis, N.; Zelilidis, A.; Collins, W.J. Hydrocarbon generating potential of a Lower Permian sedimentary succession (Mount Agony Formation): Southern Sydney Basin, New South Wales, Southeast Australia. *Int. J. Coal Geol.* **2017**, *83*, 52–64. [CrossRef]
4. Wang, X.; He, S.; Wu, J. Tectonic controls on lacustrine source rock occurrence in the Huizhou Sag, Pearl River Mouth Basin, China. *Int. Geol. Rev.* **2020**, *62*, 72–93. [CrossRef]
5. Maravelis, A.G.; Catuneanu, O.; Nordsvan, A.; Landenberger, B.; Zelilidis, A. Interplay of tectonism and eustasy during the Early Permian icehouse: Southern Sydney Basin, southeast Australia. *Geol. J.* **2018**, *53*, 1372–1403. [CrossRef]
6. Shehata, A.A.; El Fawal, F.M.; Ito, M.; Abdel Aal, M.H.; Sarhan, M.A. Sequence stratigraphic evolution of the syn-rift early cretaceous sediments, west Beni Suef basin, the Western Desert of Egypt with remarks on its hydrocarbon accumulations. *Arab. J. Geosci.* **2018**, *11*, 313–331. [CrossRef]
7. Contreras, J.; Scholz, C.H. Evolution of stratigraphic sequences in multisegmented continental rift basins: Comparison of computer models with the basins of the East African rift system. *AAPG Bull.* **2001**, *85*, 1565–1581.
8. Martins-Neto, M.A.; Pedrosa-Soares, A.C.; Lima, S.A.A. Tectono-sedimentary evolution of sedimentary basins from Late Paleoproterozoic to Late Neoproterozoic in the Sao Francisco craton and Aracuai Fold belt, eastern Brazil. *Sediment. Geol.* **2001**, *141–142*, 343–370. [CrossRef]
9. Vail, P.R.; Mitchum, R.M.; Thompson, S. Global cycles of relative changes of sea level. *AAPG Bull.* **1977**, *26*, 99–116.
10. Posamentier, H.W.; Allen, G.P. Variability of the sequence stratigraphic model: Effects of local basin factors. *Sediment. Geol.* **1993**, *86*, 91–109. [CrossRef]
11. Bahroudi, A.; Koyi, H.A. Tectono-sedimentary framework of the Gachsaran Formation in the Zagros foreland basin. *Mar. Pet. Geol.* **2004**, *21*, 1295–1310. [CrossRef]
12. Lin, C.S.; Erikoson, K.; Li, S.T.; Wan, Y.X.; Ren, J.Y.; Zhang, Y.M. Sequence architecture, depositional systems and their controls of lacustrine sequence of the Erlian Basin. *AAPG Bull.* **2001**, *85*, 2017–2043.
13. Zecchin, M.; Catuneanu, O. High-resolution sequence stratigraphy of clastic shelves III: Applications to reservoir geology. *Mar. Pet. Geol.* **2015**, *62*, 161–175. [CrossRef]
14. Jackson, C.; Gawthorpe, R.L.; Carr, I.D.; Sharp, I.R. Normal faulting as a control on the stratigraphic development of shallow marine syn-rift sequences: The Nukhul and Lower Rudeis Formations, Hammam Faraun fault block, Suez Rift, Egypt. *Sedimentology* **2005**, *52*, 313–338. [CrossRef]
15. Escalona, A.; Mann, P. Tectonics, basin subsidence mechanisms, and paleogeography of the Caribbean-South American plate boundary zone. *Mar. Pet. Geol.* **2011**, *28*, 8–39. [CrossRef]
16. Wang, G.; Wang, H.; Gan, H.; Liu, E.; Xia, C.; Zhao, Y.; Chen, S.; Zhang, C. Paleogene tectonic evolution controls on sequence stratigraphic patterns in the Fushan Sag, Northern South China Sea. *J. Earth Sci.* **2016**, *27*, 654–669. [CrossRef]
17. He, J.; Wang, H.; Jiang, T.; Liu, E.; Chen, S.; Jiang, P. Sedimentary Characteristics of Lacustrine Beach-Bars and Their Formation in the Paleogene Weixinan Sag of Beibuwan Basin, Northern South China Sea. *Energies* **2022**, *15*, 3391. [CrossRef]
18. Shehata, A.A.; El Fawal, F.M.; Ito, M.; Aboulmagd, M.A.; Brooks, H.L. Senonian platform-to-slope evolution in the tectonically-influenced Syrian Arc sedimentary belt: Beni Suef Basin, Egypt. *J. Afr. Earth Sci.* **2020**, *170*, 103934. [CrossRef]
19. Sakran, S.; Shehata, A.A.; Osman, O.; El Sherbiny, M. Superposed tectonic regimes in West Beni Suef basin, Nile Valley, Egypt: Implications to source rock maturation and hydrocarbon entrapment. *J. Afr. Earth Sci.* **2019**, *154*, 1–19. [CrossRef]
20. Carroll, A.R.; Bohacs, K.M. Stratigraphic classification of ancient lakes: Balancing tectonic and climatic controls. *Geology* **1999**, *27*, 99–102. [CrossRef]
21. Feng, Y.L.; Li, S.T.; Lu, Y.C. Sequence stratigraphy and architectural variability in late Eocene lacustrine strata of the Dongying depression, Bohai Bay Basin, eastern China. *Sediment. Geol.* **2013**, *295*, 1–26. [CrossRef]
22. Zhang, Y.; Zhang, L.; Mi, L.; Lu, X.; Wu, S.; Tang, L.; Zhou, J.; Xiong, X.; Zhu, J. Quantitative Analysis of Cenozoic Extension in the Qiongdongnan Basin, South China Sea: Insight on Tectonic Control for Hydrocarbon Reservoir Accumulation and Formation. *Energies* **2022**, *15*, 4011. [CrossRef]
23. Shehata, A.A.; El Fawal, F.M.; Ito, M.; Abdel Aal, M.H.; Sarhan, M.A. Cenomanian–Turonian depositional history of a post-Gondwana rift succession in the west Beni Suef basin, Egypt. *J. Afr. Earth Sci.* **2019**, *150*, 783–798. [CrossRef]

24. Kassem, A.A.; Osman, O.; Nabawy, B.; Baghdady, A.; Shehata, A.A. Microfacies analysis and reservoir discrimination of channelized carbonate platform systems: An example from the Turonian Wata Formation, Gulf of Suez, Egypt. *J. Pet. Sci. Eng.* **2022**, *212*, 110272. [CrossRef]
25. Shanley, K.W.; McCabe, P.J. Perspectives on the sequence stratigraphy of continental strata. *AAPG Bull.* **1994**, *78*, 544–568.
26. Chen, S.; Steel, R.; Wang, H.; Zhao, R.; Olariu, C. Clinoform growth and sediment flux into late Cenozoic Qiongdongnan shelf margin, South China Sea. *Basin Res.* **2020**, *32*, 302–319. [CrossRef]
27. Xu, J.; Zhao, N.; Xu, S.; Zhao, X. Main controlling factors and development model of the Miocene marine source rocks in Yinggehai Basin. *Bull. Geol. Sci. Technol.* **2021**, *40*, 54–63.
28. Young, M.J.; Gawthorpe, R.L.; Sharp, I.R. Architecture and evolution of syn-rift clastic depositional systems towards the tip of a major fault segment, Suez Rift, Egypt. *Basin Res.* **2015**, *14*, 1–23. [CrossRef]
29. Willan, R.C.R.; Hunter, M.A. Basin evolution during the transition from continental rifting to subduction: Evidence from the lithofacies and modal petrology of the Jurassic Latady Group, Antarctic Peninsula. *J. S. Am. Earth Sci.* **2005**, *20*, 171–191. [CrossRef]
30. Elliott, W.S.J.; Suttner, L.J.; Pratt, L.M. Tectonically induced climate and its control on the distribution of depositional systems in a continental foreland basin, Cloverly and Lakota Formations (Lower Cretaceous) of Wyoming, U.S.A. *Sediment. Geol.* **2007**, *202*, 730–753. [CrossRef]
31. Liu, E.; Wang, H.; Feng, Y.; Pan, S.; Jing, Z.; Ma, Q.; Gan, H.; Zhao, J. Sedimentary architecture and provenance analysis of a sublacustrine fan system in a half-graben rift depression of the South China Sea. *Sediment. Geol.* **2020**, *409*, 105781. [CrossRef]
32. Nottvedt, A.; Gabrielsen, R.H.; Steel, R.J. Tectonostratigraphy and sedimentary architecture of rift basins, with reference to the northern North Sea. *Mar. Pet. Geol.* **1995**, *12*, 881–901. [CrossRef]
33. Liu, E.; Wang, H.; Li, Y.; Zhou, W.; Leonard, N.D.; Lin, Z.; Ma, Q. Sedimentary characteristics and tectonic setting of sublacustrine fans in a half-graben rift depression, Beibuwan Basin, South China Sea. *Mar. Pet. Geol.* **2014**, *52*, 9–21. [CrossRef]
34. Zhou, Y.; Ji, Y.L.; Pigott, J.D.; Meng, Q.A.; Wan, L. Tectonostratigraphy of lower cretaceous tanan sub-basin, tamtsag basin, mongolia: Sequence architecture, depositional systems and controls on sediment infill. *Mar. Pet. Geol.* **2014**, *49*, 176–202. [CrossRef]
35. Wang, H.; Chen, S.; Gong, T.; Yu, Z.; Huang, C.; Zhang, Y.; Zhao, R. Sedimentary process and accumulation mechanism of traction fluidization gravity flow: An example from Qikou Sag, Bohai Bay Basin. *Bull. Geol. Sci. Technol.* **2020**, *39*, 95–104.
36. Alfaro, E.; Holz, M. Seismic geomorphological analysis of deepwater gravity-driven deposits on a slope system of the southern Colombian Caribbean margin. *Mar. Pet. Geol.* **2014**, *57*, 294–311. [CrossRef]
37. Allen, P.A. From landscapes into geological history. *Nature* **2018**, *451*, 274–276. [CrossRef]
38. Andrić, N.; Sant, K.; Matenco, L.; Mandic, O.; Tomljenović, B.; Pavelić, D.; Ooms, J. The link between tectonics and sedimentation in asymmetric extensional basins: Inferences from the study of the Sarajevo-Zenica Basin. *Mar. Pet. Geol.* **2017**, *83*, 305–332. [CrossRef]
39. Prather, B.E. Controls on reservoir distribution, architecture and stratigraphic trapping in slope settings. *Mar. Pet. Geol.* **2003**, *20*, 529–545. [CrossRef]
40. Liu, E.; Wang, H.; Li, Y.; Leonard, N.D.; Feng, Y.; Pan, S.; Xia, C. Relative role of accommodation zones in controlling stratal architectural variability and facies distribution: Insights from the Fushan Depression, South China Sea. *Mar. Pet. Geol.* **2015**, *68*, 219–239. [CrossRef]
41. Khalil, S.M.; Mc Clay, K.R. Structural control on syn-rift sedimentation, northwestern Red Sea margin, Egypt. *Mar. Pet. Geol.* **2009**, *26*, 1018–1034. [CrossRef]
42. Yang, X.B.; Chang, L.; Xu, R.; Cheng, D.X.; Yin, Z.J.; You, J.J.; Liu, K.; Hu, G.W. Types and sand control effect of terrestrial slope breaks of Wenchang Sag inside the Pearl River Mouth Basin. *Earth Sci.* **2020**, *45*, 989–997, (In Chinese with English Abstract).
43. Pei, J.; Zhang, C.; Wang, Y.; Wang, K.; Liu, J.; Wang, S. Tectonic evolution and depositional response in southern continental marginal basins of South China Sea during period of rift- drift-foreland: A case study from the Liyue Basin. *Bull. Geol. Sci. Technol.* **2021**, *40*, 42–53.
44. Xie, Y. Sedimentary characteristics and hydrocarbon exploration potential of the upstream of the Central Canyon in the Yinggehai and Qiongdongnan basins. *Bull. Geol. Sci. Technol.* **2020**, *39*, 69–78.
45. Liu, Y.; Chen, H.; Wang, Y.; Han, J.; Li, Q. Diagenetic effect of mantle-derived CO_2 charge to clay minerals in the Baiyun-Liwan deepwater area of the Pearl River Mouth Basin, the South China Sea. *Bull. Geol. Sci. Technol.* **2021**, *40*, 85–95.
46. Huang, B.; Xiao, X.; Zhang, M. Geochemistry, grouping and origins of crude oils in the western Pearl River Mouth Basin, offshore south China sea. *Org. Geochem.* **2003**, *34*, 993–1008. [CrossRef]
47. Quan, Y.; Liu, J.; Zhao, D.; Hao, F.; Wang, Z.; Tian, J. The origin and distribution of crude oil in Zhu III sub-basin, Pearl River Mouth Basin. China. *Mar. Petrol. Geol.* **2015**, *66*, 732–747. [CrossRef]
48. Dong., D.D.; Zhang, G.C.; Zhong, K.; Yuan, S.Q.; Wu, S.G. Tectonic evolution and dynamics of deep water area of Pearl River Mouth Basin, Northern South China Sea. *J. Earth Sci.* **2009**, *20*, 47–159. [CrossRef]
49. Xie, H.; Zhou, D.; Li, Y.; Pang, X.; Li, P.; Chen, G.; Li, F.; Cao, J. Cenozoic tectonic subsidence in deepwater sags in the Pearl River Mouth Basin, northern South China sea. *Tectonophysics* **2014**, *615–616*, 182–198. [CrossRef]

50. Liu, E.; Chen, S.; Yan, D.; Deng, Y.; Wang, H.; Jing, Z.; Pan, S. Detrital zircon geochronology and heavy mineral composition constraints on provenance evolution in the western Pearl River Mouth basin, northern south China sea: A source to sink approach. *Mar. Pet. Geol.* **2022**, *145*, 105884. [CrossRef]
51. Tang, X.; Yang, S.; Zhu, J.; Long, Z.; Jiang, G.; Huang, S.; Hu, S. Tectonic subsidence of the Zhu 1 sub-basin in the Pearl River Mouth Basin, northern South China Sea. *Front. Earth Sci.* **2017**, *11*, 729–739. [CrossRef]
52. Gong, Z.; Li, S.; Xie, T.; Zhang, Q.; Xu, S.; Xia, K.; Yang, J.; Sun, Y.; Liu, L. *Continental Margin Basin Analyss and Hydrocarbon Accumulation of the Northern South China Sea*; China Science Press: Beijing, China, 1997.
53. Wang, Y.; Zhao, Y.; Ding, W.; Fang, P.; Li, J. Cenozoic propagated rifting in the dangerous grounds in response to the episodic seafloor spreading of the South China Sea. *J. Earth Sci.* **2022**, *33*, 1031–1046. [CrossRef]
54. Tian, L.X. Sedimentary-reservoir characteristics under control of transfer modeland implications for hydrocarbon exploration in huizhou depression, Pearl River Mouth Basin. *Earth Sci.* **2021**, *46*, 4043–4056.
55. Guo, W.; Xu, G.Q.; Liu, B.J.; Xiang, X.H.; Liu, D.Q.; Zhang, B. Structure-sedimentary response relationship of Wenchang Formation in Baiyun Sag, Pearl River Mouth Basin. *Earth Sci.* **2022**, *47*, 2433–2453.
56. Wu, J.; Zhang, X.; Bai, H.; Zheng, X.; Cai, G.; Li, Z. Miocene tidal control system and its exploration significance of lithologic trap in Yangjiang Sag, Pearl River Mouth Basin. *Earth Sci.* **2021**, *46*, 3673–3689.
57. He, Z.; Yin, X.; Jiang, S.; Lei, M.; Liu, Y.; Zhao, R.; Zhu, B. Source rock classification, maturity and their implications in paleoenvironment reconstruction in the Zhu III sub-basin, China. *J. Pet. Sci. Eng.* **2022**, *216*, 110799. [CrossRef]
58. Catuneanu, O. Model-independent Sequence Stratigraphy. *Earth-Sci. Rev.* **2019**, *188*, 312–388. [CrossRef]
59. Maravelis, A.; Boutelier, D.; Catuneanu, O.; Seymour, K.; Zelilidis, A. A review of tectonics and sedimentation in a forearc setting: Hellenic Thrace Basin, north Aegean Sea and mainland Greece. *Tectonophysics* **2016**, *674*, 1–19. [CrossRef]
60. Catuneanu, O.; Zecchin, M. Unique vs. non-unique stratal geometries: Relevance to sequence stratigraphy. *Mar. Pet. Geol.* **2016**, *78*, 184–195. [CrossRef]
61. Breckenridge, J.; Maravelis, A.G.; Catuneanu, O.; Ruming, K.; Holmes, E.; Collins, W.J. Outcrop analysis and facies model of an Upper Permian tidally influenced fluvio-deltaic system: Northern Sydney Basin, Southeast Australia. *Geol. Mag.* **2019**, *156*, 1715–1741. [CrossRef]
62. Melehan, S.; Botziolis, C.; Maravelis, A.G.; Catuneanu, O.; Ruming, K.; Holmes, E.; Collins, W.J. Sedimentology and Stratigraphy of an Upper Permian Sedimentary Succession: Northern Sydney Basin, Southeastern Australia. *Geosciences* **2021**, *11*, 273. [CrossRef]
63. Liu, E.; Wang, H.; Pan, S.; Qin, C.; Jiang, P.; Chen, S.; Yan, D.; Lü, X.; Jing, Z. Architecture and depositional processes of sublacustrine fan systems in structurally active settings: An example from Weixinan Depression, northern South China Sea. *Mar. Pet. Geol.* **2021**, *134*, 105380. [CrossRef]
64. Gawthorpe, R.L.; Leeder, M.R. Tectono-sedimentary evolution of active extensional basins. *Basin Res.* **2000**, *12*, 195–218. [CrossRef]
65. Schlische, R.W. Half-graben filling models: Implications for the evolution of continental extensional basins. *Basin Res.* **1991**, *3*, 123–141. [CrossRef]
66. Ge, J.; Zhao, X.; Tan, M.; Zhuo, H.; Liu, C.; Jones, B.G. Sequence stratigraphy and depositional evolution of the north-eastern shelf (33.9–10.5 Ma) of the Pearl River Mouth basin, South China Sea. *Mar. Pet. Geol.* **2022**, *141*, 105697. [CrossRef]
67. Ravnås, R.; Steel, R.J. Architecture of marine rift-basin successions. *AAPG Bull.* **1998**, *82*, 110–146.
68. Cai, Q.; Hu, M.; Ngia, N.R.; Hu, Z. Sequence stratigraphy, sedimentary systems and implications for hydrocarbon exploration in the northern Xujiaweizi Fault Depression, Songliao Basin, NE China. *J. Pet. Sci. Eng.* **2017**, *152*, 471–494. [CrossRef]
69. Khalifa, M.K.; Mills, K.J. Predicting sequence stratigraphic architecture and its implication for hydrocarbon reservoir potential of the uppermost Silurian through Lower Devonian Winduck Interval, central Darling Basin of western New South Wales, SE Australia. *Mar. Pet. Geol.* **2022**, *142*, 105725. [CrossRef]
70. Li, H.; Wu, J.; Huang, J.; Wang, Y.; Li, Z. Quantitative analysis of fault vertical sealing ability and its application in an Oilfield of Bohai Bay Basin. *Bull. Geol. Sci. Technol.* **2020**, *39*, 125–131.
71. Cheng, P.; Tian, H.; Huang, B.; Wilkins, R.W.T.; Xiao, X. Tracing early-charged oils and exploration directions for the Wenchang a sag, western Pearl River Mouth Basin, offshore south China sea. *Org. Geochem.* **2013**, *61*, 15–26. [CrossRef]